Application of Adaptive Network Fuzzy Inference System to Die Shape Optimal Design in Sheet Metal Bending Process

Fung-Huei Yeh*, Ching-Lun Li and Kun-Nan Tsay

Department of Mechanical and Electro-Mechanical Engineering, Tamkang University, Tamsui, Taiwan 251, R.O.C.

Abstract

This paper combines adaptive network fuzzy inference system (ANFIS) and finite element method (FEM) to study the die shape optimal design in sheet metal bending process. At first, the explicit dynamic FEM is used to simulate the sheet metal bending process. After the bending process, the springback is analyzed by using the implicit static FEM to establish the basic database for ANFIS. Then, the die shape optimal design is performed by ANFIS using this database in the sheet metal bending process. As a verification of this system, the L-type and V-type dies are designed for the experiments to prove the reliability of FEM analysis and ANFIS optimal design by comparing the punch load and stroke relationship, the deformation history, stress distribution, and the bending angle of workpiece after springback between numerical and experimental results. It shows that a good agreement is achieved from comparison between numerical and experimental results. From this investigation, ANFIS has proved to be a useful scheme for die shape optimal design in the metal forming category.

Key Words: Adaptive Network Fuzzy Inference System, Finite Element Method, Die Shape Optimal Design, Springback, Sheet Metal Bending Process

1. Introduction

Sheet metal bending is one of the most widely used industrial forming operations, especially for household appliances, automobile, shipbuilding, aircraft, packaging, and the furniture industry. Specific examples of sheet metal bending products are pet food containers, beverage cans, razor caps, housings, stiffeners, cars bodies, and outer and inner panels. The elastic redistribution of sheet metal occurs due to the unloading when sheet metal is removed from the die. Springback is a common phenomenon in sheet metal bending process. The amount of springback affects the precision and assembly of the product due to the error between the objective and the final shape. Interplay of these factors causes springback prediction to be especially complicated and difficult to investigate. Springback is mainly affected by thickness of sheet metal, material parameters, and the punch and die profile radius [1,2]. The cracking and dimension accuracy in U-shaped part forming can be improved by reasonable variable blankholder force [3]. Chan et al. [4] studied the springback angles of the workpiece in V-bending by varying the punch angle, punch radius and die-lip radius. A die design recommendation for one material AL2024-T4 is conducted to reduce springback [5].

There are two common methods used to prevent springback and satisfy the specification of the product, minimizing springback or compensating for the profile of the mold. Lin and Tai [6] established a predictive model of the neural network to find the bend parameters with minimum springback in L-shaped bend. For the compensation of springback in die shape optimal design, Gan and Wagoner [7] considered springback in propos-

*Corresponding author. E-mail: funghuei@mail.tku.edu.tw

ing a new die design method (displacement adjustment method) to produce a desired final part shape. It usually need a few iterations, and may oscillate in convergence behavior. Furthermore, Sousa et al. [8] coupled a genetic algorithm (FORTRAN codes) and the commercial software ABAQUS for search the optimal geometry of tools. It spent much time to find the best combination of design variables.

To reduce effectively the time and cost in designing the product, adaptive network fuzzy inference system (ANFIS) [9], using hybrid-learning procedure to construct a set of fuzzy if-then rules with appropriate membership functions to generate the stipulated input-output pairs, has served as another valuable approach to the metal forming process. ANFIS has been applied to inverse prediction of hole profile in the hole bore-expanding [10,11] and optimization of blank design in stretch flange process [12]. But, ANFIS has not been applied to the die shape optimal design in sheet metal bending process yet.

This study presents a prediction scheme that combines the finite element method (FEM) and ANFIS to determine the die shape optimal design in L-bending and V-bending processes. The explicit dynamic FEM and implicit static FEM are used to analyze the bending process and springback respectively. The die shape optimal design of the bending process can be inversely determined efficiently using ANFIS. To verify the accuracy of ANFIS, a set of optimal V-bending die are designed to perform the experiment. From comparison of the results between simulation and experiment, ANFIS can accurately calculate the exact optimal die shape in sheet metal bending process. This scheme can be also easily applied to predict the optimal die shape in other metal forming processes.

2. Basic Theory

2.1 Explicit Dynamic Finite Element Method

In the framework of the explicit dynamic finite element method, the virtual work governing equation that involves internal force, body force, contact force, and momentum can be expressed as follows [13]:

$$\int_V \rho \ddot{\mathbf{x}} \delta \mathbf{x} dV + \int_V \sigma \delta \varepsilon dV - \int_V \rho \mathbf{b} \delta \mathbf{x} dV - \int_S \mathbf{f} \delta \mathbf{x} dS = 0 \qquad (1)$$

where $\ddot{\mathbf{x}}$ is the acceleration, σ is the Cauchy stress, ε is the strain, ρ is the mass density, **b** is the body force density, and f denotes the surface traction force. After the finite element discretion, Eq. (1) is described in a matrix form as the following:

$$\mathbf{M}\ddot{\mathbf{u}} = \mathbf{F}_t^1 + \mathbf{F}_t^2 + \mathbf{F}_t^3 \qquad (2)$$

where **M** is the mass matrix, $\mathbf{F}_t^1$, $\mathbf{F}_t^2$ and $\mathbf{F}_t^3$ are the stress load, body force load, and surface force load at time t respectively, and N is the shape function. The solution for time $t + \Delta t$ can be obtained by solving the acceleration $\ddot{\mathbf{u}}$ in Eq. (2). The central difference method is then used to calculate velocity and displacement as follows:

$$\ddot{\mathbf{u}}_t = \mathbf{M}^{-1}(\mathbf{F}_t^1 + \mathbf{F}_t^2 + \mathbf{F}_t^3) \qquad (3)$$

$$\mathbf{v}_{t+\Delta t/2} = \mathbf{v}_{t-\Delta t/2} + \ddot{\mathbf{u}}_t \Delta t_t \qquad (4)$$

$$\mathbf{u}_{t+\Delta t} = \mathbf{u}_t + \mathbf{v}_{t+\Delta t/2} \Delta t_{t+\Delta t/2} \qquad (5)$$

where $\Delta t_{t+\Delta t/2} = (\Delta t_t + \Delta t_{t+\Delta t})/2$, and v and u are the nodal velocity and displacement. The time increment Δt in the central difference method should be smaller than a critical time increment Δt_{cri} to guarantee the convergence in the solution procedure; and the critical time increment Δt_{cri} for the shell element in the explicit dynamic scheme is decided from the following equation:

$$\Delta t_{\text{cri}} = \frac{L_s}{\sqrt{E/\rho(1-\nu^2)}} \qquad (6)$$

where L_s is the characteristic length calculated from the element area divided by the longest side in the element. E and ν are the Young's modulus and Poisson's ratio, respectively. As each element has its critical time increment, the critical time increment in a deformation stage is determined by the minimum value in the whole system, that is,

$$\Delta t_{t+\Delta t} = \alpha \min\{\Delta t_1, \Delta t_2, \cdots, \Delta t_n\} \qquad (7)$$

where n denotes the element number. Δt_i is the critical time increment for element i, and α is a safety parameter, which is usually set at 0.9 in the simulation. It is apparent that the time increment in Eq. (6) is proportional to the square root of the mass density. Hence, the merit of the explicit dynamic scheme is that if the simulation results still maintain the accuracy, increasing the velocity factor or the mass density factor is allowable to save the execution time in the simulation.

2.2 Implicit Static Finite Element Method

In the implicit static finite element method, the acceleration and velocity term are neglected, the principle of virtual work leads to

$$\mathbf{Ku} = \mathbf{R} = \mathbf{F}_{n+1}^{\text{ext}} - \mathbf{F}_{n}^{\text{int}} \tag{8}$$

where **K** is the stiffness matrix, **u** is the nodal displacement, **R** is the load vector from the out-of-balance internal stresses, $\mathbf{F}_{n+1}^{\text{ext}}$ is the nodal external force, and $\mathbf{F}_{n}^{\text{int}}$ is the nodal internal force. In the implicit static finite element method, the nodal displacement can be solved as follows:

$$\mathbf{u} = \mathbf{K}^{-1}(\mathbf{F}_{n+1}^{\text{ext}} - \mathbf{F}_{n}^{\text{int}}) \tag{9}$$

The stiffness matrix formed during implicit analysis requires a large amount of memory, and computing the inverse requires most of the solution time. In the static analysis, no confirmation is performed to ensure that the resulting springback produced balanced internal stresses. Thus, the static approach yields inaccurate results and should only be used to estimate springback.

2.3 Adaptive-Network-Based Fuzzy Inference System

2.3.1 Architecture of the ANFIS

The adaptive-network-based fuzzy inference system (ANFIS) [9] can simulate and analyze the mapping relationship between the input and output data through hybrid learning to determine optimal distribution of membership function. This particular ANFIS is based mainly on the fuzzy "if-then" rules from the Takagi and Sugeno's type [14], and involves a premise and consequent. The equivalent ANFIS architecture of Takagi and Sugeno's type, as shown in Figure 1, comprises five layers in this inference system. Each layer involves several nodes, which are described by the node function. The output signals from nodes in the previous layers will be accepted as the input signals in the present layer. The output serves as input signals for the next layer after manipulation by the node function in the present layer. Here, square nodes, called "adaptive nodes", are adopted to demonstrate that the parameter sets in these nodes are adjustable. Whereas, circle nodes, named "fixed nodes", are adopted to demonstrate that the parameter sets are fixed in the system. To explain the procedure of the ANFIS simply two inputs, x and y, and one output, f, are included in the fuzzy inference system. In the first order of the Sugeno fuzzy inference model, the typical fuzzy "if-then" rules can be expressed as:

Rule 1: if x is A_1 and y is B_1 then $f = p_1x + q_1y + r_1$

Rule 2: if x is A_2 and y is B_2 then $f = p_2x + q_2y + r_2$

The five layers in the ANFIS are fuzzy, production, normalized, defuzzy, and total output layer, in that order. The following concepts are the input and output relationships of each layer.

Layer 1: Fuzzy

Every node in this layer is an adjustable node, marked by a square node, with the node function as:

$$O_{1,i} = \mu A_i(x), \quad i = 1,2 \tag{10}$$

$$O_{1,i} = \mu B_{i-2}(y), \quad i = 3,4 \tag{11}$$

where x (or y) is the input of the node, and A_i (or B_{i-2}) is the linguistic variable. The membership function usually adopts a bell-shape with maximum and minimum equal to 1 and 0, respectively:

$$\mu(x) = \frac{1}{1 + \left| \dfrac{x - c_i}{a_i} \right|^{2b_i}} \tag{12}$$

where $\{a_i, b_i, c_i\}$ represents the parameter set. It is significant that if the values of these parameters set changes, the bell-shape function will be changed accordingly. Meanwhile, the membership functions are also different in the linguistic label A_i. The parameters in this layer are called "premise parameters".

Layer 2: Production

Every node in this layer is a fixed node and marked

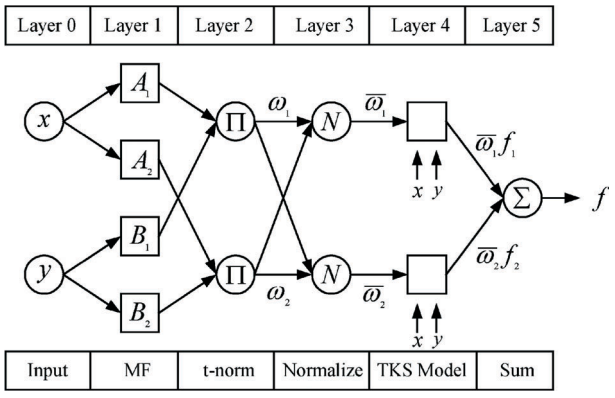

Figure 1. The architecture of ANFIS.

by a circle node with the node function multiplying input signals to serve as the output signal,

$$O_{2,i} = t(\mu_{A_i}(x), \mu_{B_i}(y)) = \mu_{A_i}(x) \times \mu_{B_i}(y) = \omega_i \quad (13)$$

The output signal ω_i meant the firing strength of a rule.

Layer 3: Normalized

Every node in this layer is a fixed node and marked by a circle node with the node function normalizing firing strength by calculating the ratio of this node firing strength to the sum of the firing strength:

$$O_{3,i} = \overline{\omega}_i = \frac{\omega_i}{\omega_1 + \omega_2} \quad (14)$$

Layer 4: Defuzzy

Every node in this layer is an adjustable node and marked by a square node with the node function as:

$$O_{4,i} = \overline{\omega}_i f_i = \overline{\omega}_i (p_i x + q_i y + r_i) \quad (15)$$

where $\overline{\omega}_i$ is the output of Layer 3. $\{p_i, q_i, r_i\}$ are the parameter set, which is referred to as the consequent parameters.

Layer 5: Total output

Every node in this node is a fixed node and marked by a circle node with the node function computing the overall output by:

$$O_{5,i} = \sum_i \overline{\omega}_i f_i = \frac{\sum_i \omega_i f_i}{\sum_i \omega_i} \quad (16)$$

Explicitly, this layer sums the node's output in the previous layer to be the output of the whole network.

2.3.2 Hybrid-Learning Algorithm

From the architecture of the ANFIS, if the parameters in the premise part are fixed, the output of the whole network system would be the linear combination of the consequent parameters.

3. Finite Element Analysis and Experiment

The planned framework of the predictive scheme for die shape optimal design in the sheet metal bending process is illustrated in Figure 2. To verify the finite element analysis, this paper designs the tools of L-bending and V-bending for the experiments. Figures 3 and 4 show the dimensions of tools and blank in the L-bending and V-bending processes.

3.1 Finite Element Analysis

The finite element analysis comprises three rigid bodies, punch, die and blank holder, and a deformable blank sheet. The element used in the simulation is SHELL 163 that adopts four nodes to represent the sheet. The blank has an original rectangular shape 80.0 mm × 35.0 mm in the L-bending process, and the finite element model involves 200 elements and 231 nodes as shown in Figure 5. Figure 6 shows the finite element mesh and boundary condition of the blank in the V-bending process, the blank is a square with diagonal of 68.0 mm. To reduce the solution time, only right half of each tool and blank is built due to the symmetrical condition. An automesh program is used to mesh the blank, and the mesh of the blank involves 1800 elements and 1861 nodes. The nodes on the Y-axis have a displacement constraint in the X direction and rotation constraint in the Y and Z directions.

To eliminate rigid body motion (three translations and three rotations), an adequate number of constraints

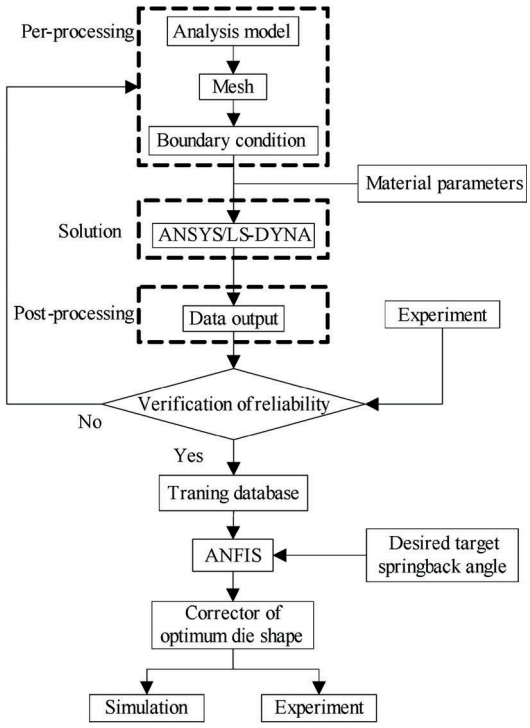

Figure 2. Proposed prediction process of ANFIS and experiment.

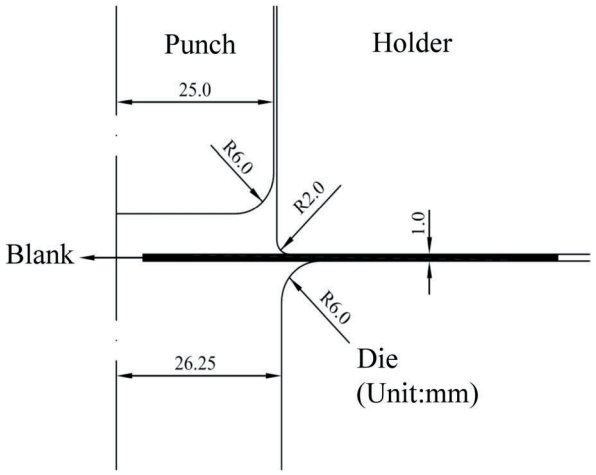

Figure 3. The dimensions of blank and die assembly in the L-bending process.

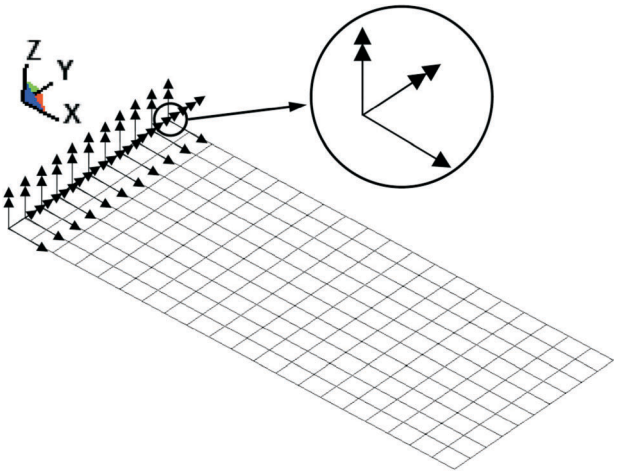

Figure 5. The finite element meshes of the blank in the L-bending process.

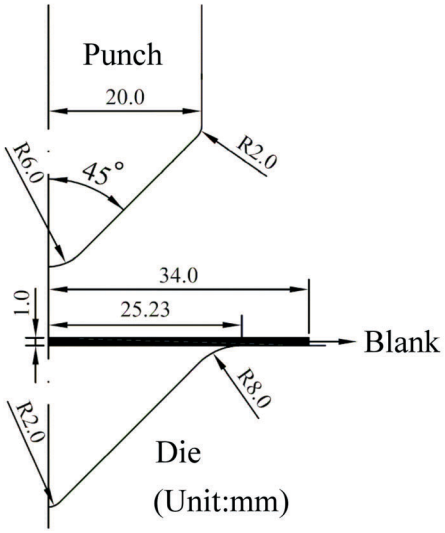

Figure 4. The dimensions of blank and die assembly in the V-bending process.

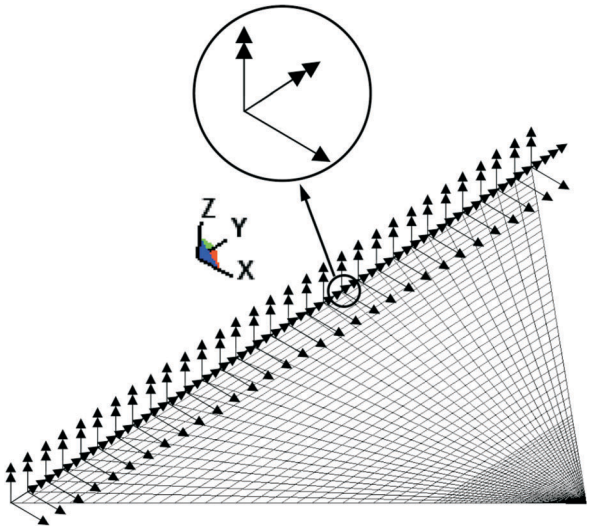

Figure 6. The finite element meshes and boundary conditions of the blank in the V-bending process.

must be defined during the springback analysis. The three constraint points should be chosen well separated from each other, and away from edges and flexible areas in the part. Figure 7 is the location of required constraints for the full model in the springback analysis. Point A is the reference point, receiving constraints to all three translational degrees of freedom. All displacements of the point A are zero dx = dy = dz = 0. Point B is located away from point A along the global X-direction. Constraints are applied at point B to eliminate global Y- and Z-translations (dy = dz = 0). Point C is located away from point A along the global Y-direction. Only the global Z-translation is constrained at point C (dz = 0). Figure 8 shows the required constraints for the symmetry model in the springback analysis. The constraints must be added to two points on the symmetry plane (Y-Z plane). All displacements of reference point A are constrained (dx = dy = dz = 0), eliminating the three translational rigid body motion of the part. In addition to the standard symmetry constraints, selected translational degrees of freedom are constrained at point B to eliminate the three rigid body rotations of the part about point A.

Aluminum 6061 used in the experiments is supplied by the China steel corporation. The materials are tested according to JIS standard test method in the direction of 0°, 45°, 90° with respect to the rolling direction. The material parameters of aluminum 6061 are as follows:
Initial thickness of blank: t_b = 1.0 mm

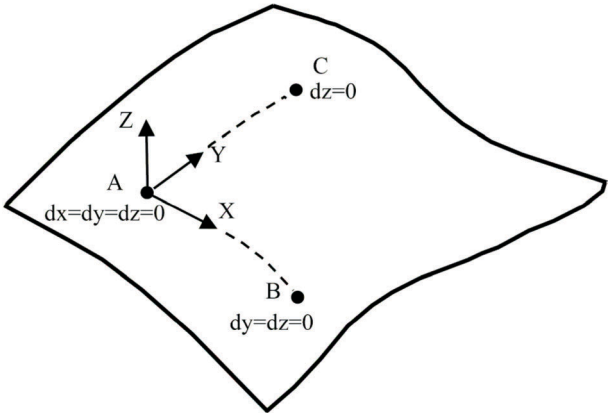

Figure 7. The location of constraint nodes for the full model in the springback analysis.

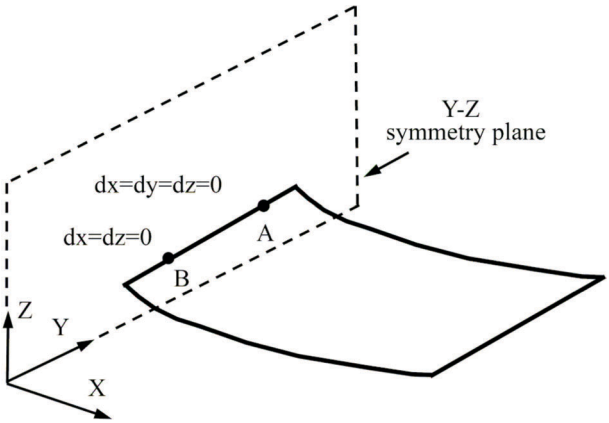

Figure 8. The location of constraint nodes for the symmetric model in the springback analysis.

Stress-strain constitutive equation: $\overline{\sigma} = 395.01(0.006104 + \bar{\varepsilon}_p)^{0.0582}$ MPa
Yield stress: $\sigma_y = 293.59$ MPa
Young's modulus: $E = 73313.8$ MPa
Lankford value: $R_0 = 0.63$, $R_{45} = 0.48$, $R_{90} = 0.84$
Poisson's ratio: $\nu = 0.3$

The Coulomb friction law is used to determine the friction coefficient between the blank and tools. The friction coefficient is set at 0.1.

3.2 Experimental Work

The experimental equipment includes a 50-ton hydraulic press forming machine and data acquisition device. The relationship between punch load and stroke during the forming process can be shown synchronously in the computer monitor through data acquisition equipment. The procedure of the experiment is summarized as follows:

(1) Assemble the tools on the hydraulic press forming machine;
(2) Adjust the center position between the punch and die;
(3) Spray uniformly a thin film of zinc stearate [$Zn(C_{18}H_{35}O_2)$] onto the contact surface between the blank and tools;
(4) Set the punch velocity and stroke for the punch to press the blank;
(5) Record the punch load-stroke relationship during the bending process;
(6) Measure the experimental bending angle of the workpiece to compare with the FEM results by using optical profile projector and digital readout.

3.3 Comparison of Numerical Analysis and Experimental Results

The present study designs the L-type and V-type dies for the expeiments of the bending process. The punch load, deformation history, stress distribution and numerical bending angle of the workpiece after springback are discussed and compared with the experimental results. The reliability of the analytical program can be proved by the comparison between simulations and experimental results.

Figure 9 shows the comparison of punch load between the simulation and experiment in the L-bending process. When the punch presses the blank downward, it causes the punch load to increase as the stroke increases until a maximal value is achieved. After the maximum

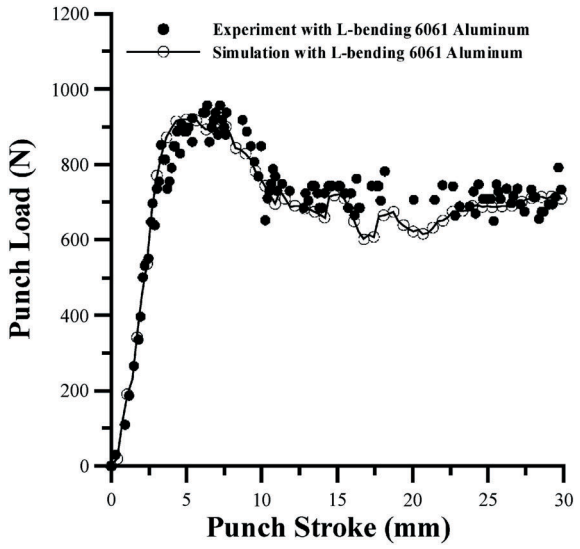

Figure 9. The comparison of punch load between simulation and experiment in L-bending process.

punch load, the punch load decreases with the increase of the stroke. When the workpiece has already bent completely, it only receives the friction between the workpiece and tools. Then, the punch load reduces to 700N and maintains steadily. Figure 10 is the deformation history and stress distribution of the workpiece in the L-bending process. The blank is bent gradually with the increase of the stroke from Figure 10 (a)–(c). The numerical bending angle of the workpiece after springback equals 99.79° in Figure 10(d). The experimental bending angle of the workpiece is 100.25° measured by two lines (Line 1 and Line 2) composed of four points (Points A, B, C, and D) in Figure 11, and the angle error between experiment and simulation is only 0.46%. As shown in Figure 12, the deformed mesh is merged into the formed shape of the workpiece to obtain a clear comparison between experiment and simulation. The simulation has good coincidence with the experimental results.

A comparison between the experimental results and simulation for punch load versus stroke in the V-bending process is shown in Figure 13. When the V-bending process starts, the punch load increases gradually due to the tip of the punch pressing the blank. The outer and inner blank are each stretched and compressed during the bending process. The punch load then maintains stably while the stroke increases. When the blank is pressed tightly by the punch and die, the punch load increases rapidly to the maximal value. It can be observed that the simulated punch load shows good coincidence with the experimental result in Figure 13. In Figure 14, the experimental bending angle of the workpiece equals 93.73° measured by two lines (Line 1 and Line 2) composed of

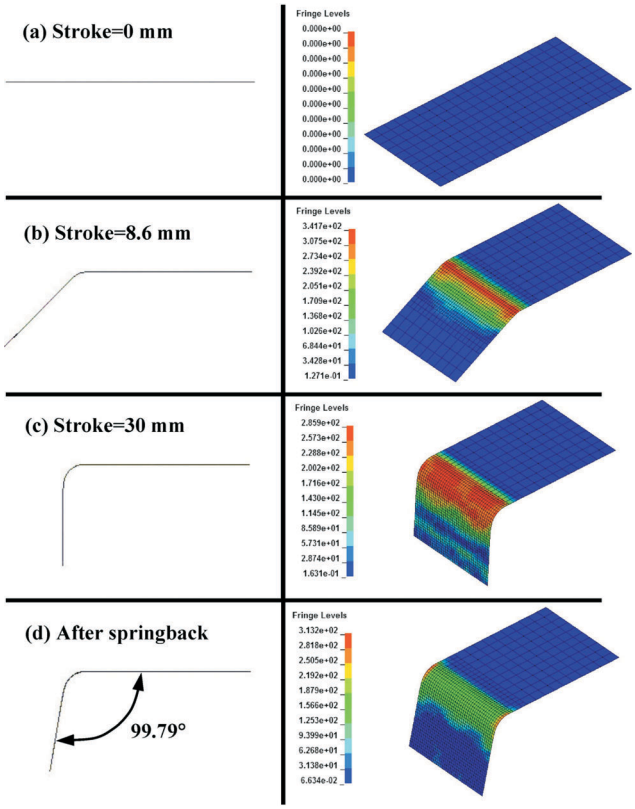

Figure 10. The deformation history and stress distribution of workpiece in the L-bending process (a, b, c, d).

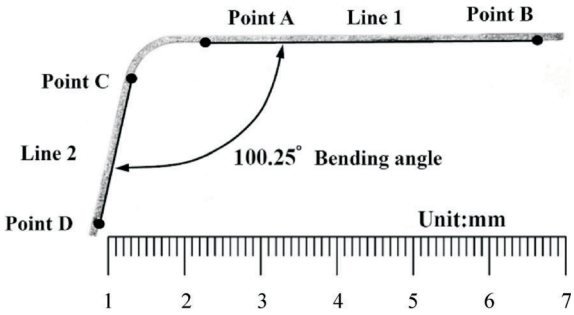

Figure 11. The workpiece for the original die shape in the L-bending process.

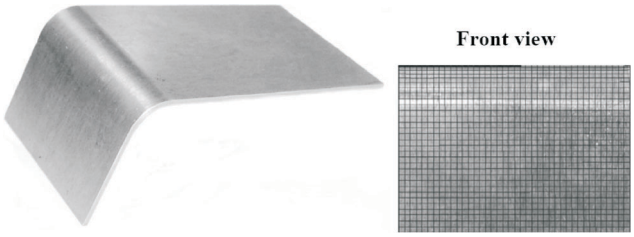

Figure 12. Photograph of deformed mesh and formed shape of the workpiece in the L-bending process.

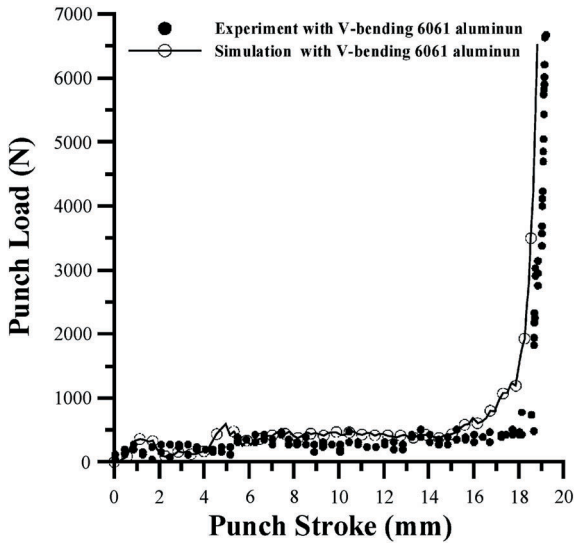

Figure 13. The comparison of punch load between simulation and experiment in V-bending process.

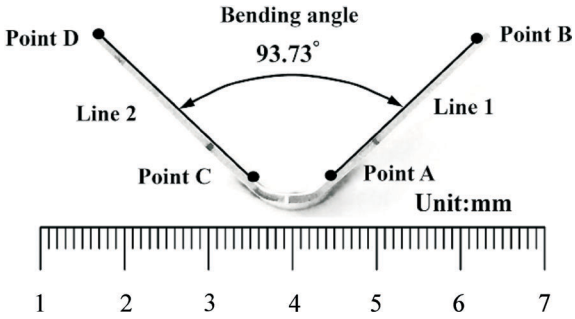

Figure 14. The workpiece for the original die shape in the V-bending process.

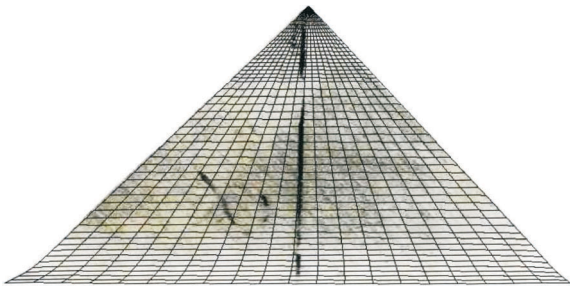

Figure 15. Photograph of deformed mesh and formed shape of the workpiece in the V-bending process.

four points (Points A, B, C, and D) when the angle of the original die is 90.00°. The numerical and experimental bending angles of the workpieces are 93.83° and 93.73°. The angle error between experiment and simulation is only 0.11%. In Figure 15, the deformed mesh of FEM is merged into the formed shape of the workpiece. The deformed mesh gives a satisfactory agreement with the experimental formed shape.

4. Die Shape Optimal Design in the L-Bending and V-Bending

4.1 Die Shape Optimal Design

This paper adopts five bell-shape membership functions and 200 hybrid-learning cycles to formulate the knowledge rule database in ANFIS training. The angle of die and bending angle of the workpiece are adopted as the input data of the knowledge rule database. The range of die angle are 90°~95° (L-bending) and 80°~90° (V-bending) respectively. For ascertaining the validity of the ANFIS, the above experimental bending angles of the workpieces of 100.25° and 93.73° in L-bending and V-bending are set as the objective bending angles. Then, the die angles of 89.93° and 89.86° can be accurately obtained by the inverse prediction scheme of ANFIS. The designed die angle errors in L-bending and V-bending with above original experimental die angles are 0.077% and 0.155% respectively. ANFIS has proved to be a useful scheme for die shape optimal design in sheet metal bending process.

Next, another die shape optimal designs in the L-bending and V-bending are carried out. When the objective bending angles of workpieces of 105.00° and 90.00° in L-bending and V-bending are set, the exact optimal die shape with the die angles of 93.75° and 85.14° for the L-bending and V-bending are predicted after building the ANFIS. The numerical bending angles of the respective workpiece are equal to 104.97° and 85.14° when the angles of optimal die shape are 93.75° and 85.14° in the L-bending and V-bending processes.

Figure 16 shows the deformation history and stress distribution of the workpiece with various strokes for the optimal die shape in the L-bending process. Figure 16(a) is the initial blank. When the bending process starts, the punch makes contact and presses the blank. The blank is bent at the die radius, as shown in Figure 16(b). The maximum stress is occured at the bending position in Figure 16(c). After springback, the numerical bending angle of workpiece is approximately 104.97° as shown in Figure 16(d).

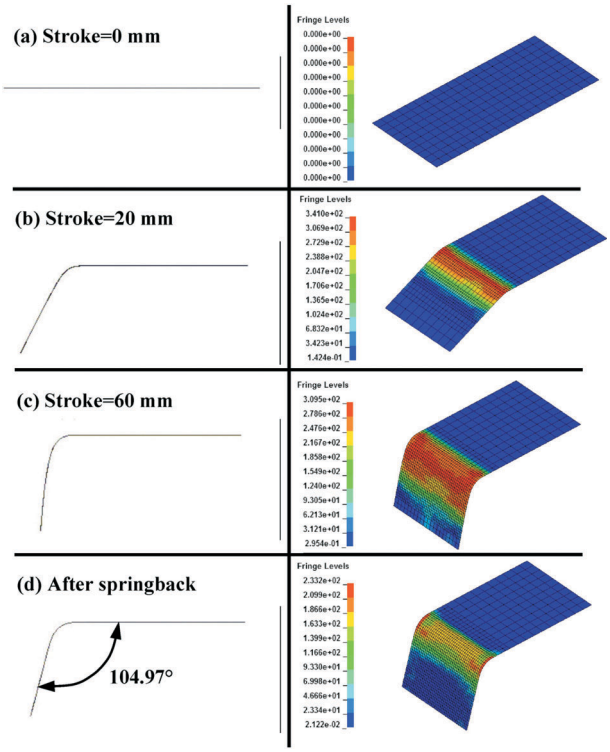

Figure 16. The deformation history and stress distribution of optimal workpiece in the L-bending process (a, b, c, d).

4.2 Comparison of Numerical Analysis and Experiment Results for the Optimal Die Shape in the V-Bending Process

To prove the reliability and accuracy of the ANFIS, the optimal die shape is designed for the experiment. The comparison between the experimental results and simulation for punch load versus punch stroke for the optimal die shape in the V-bending process is shown in Figure 17. The punch load increases slowly with the increase of stroke until the bent blank becomes tangent to the die face. The pressing process at the final bending stage causes the punch load to increase at an even steeper rate.

To understand the bending and springback processes, Figure 18 shows the deformation history and stress distribution of the workpiece with various punch strokes for the optimal die shape in the V-bending process. The numerical bending angle of the workpiece is 89.97°. The experimental bending angle of the workpiece for the optimal die shape is 89.93° in Figure 19. In Table 1, the numerical and experimental bending angles of workpieces are very close to the objective bending angle of 90°.

5. Conclusion

This paper has used the explicit dynamic and implicit static finite element methods to analyze the springback in the L-bending and V-bending processes, and used ANFIS to achieve the die shape optimal design in sheet metal bending process. By employing the hybrid-learning algorithm, ANFIS can obtain the optimal distributed membership functions to describe the mapping relation in the input process parameters and output process parameters. When the objective bending angle of workpiece is 105.00° in the L-bending process, the ANFIS predicts the angle of the L-type die to be 93.75°. The numerical bending angle of the workpiece is 104.97°. When the objective bending angle of workpiece is 90.00° in the V-bending process, the ANFIS predicts the angle of V-type die to be 85.14°. The numerical and experimental bending angles of the workpieces are 89.97° and 89.93° respectively. The deviation of the bending angle

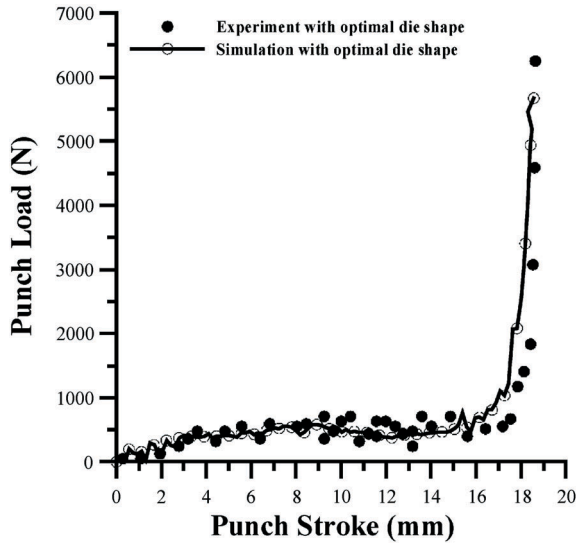

Figure 17. Comparison of punch load versus stroke for the optimal die shape in the V-bending process.

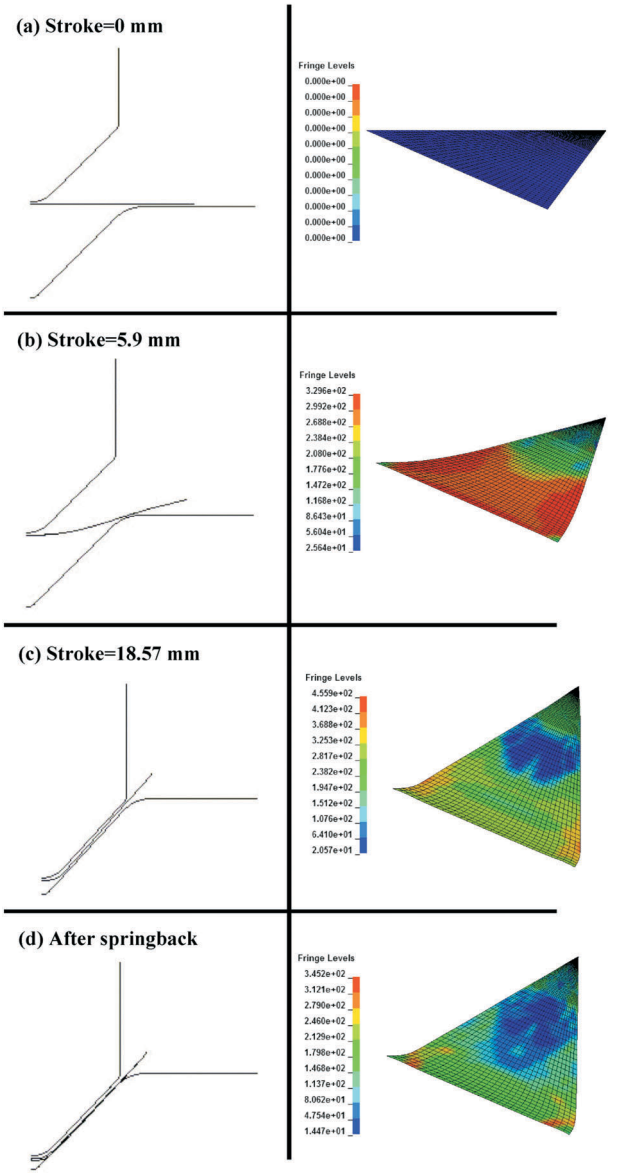

Figure 18. The deformation history and stress distribution of optimal workpiece in the V-bending process (a, b, c, d).

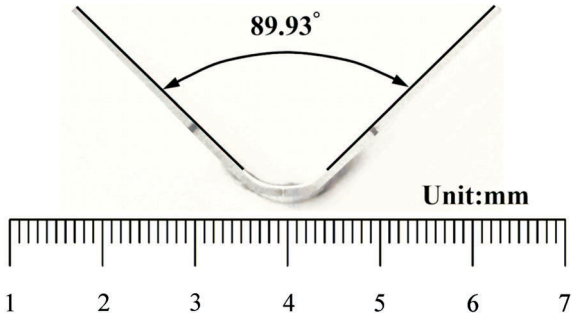

Figure 19. The workpiece for the optimal die shape in the V-bending process.

Table 1. The bending angle of workpiece for the original and optimal die shape in the V-bending process

Objective bending angle 90.00°	Bending angle of workpiece	
	Simulation	Experiment
Angle of original die 90.00°	93.83°	93.73°
Angle of optimal die 85.14°	89.97°	89.93°

is 0.044%. From the investigations, it proves that ANFIS will supply a useful die shape optimal design scheme in the metal forming industry.

References

[1] Forcellese, A., Fratini, L., Gabrielli, F. and Micari, F., "Computer Aided Engineering of Sheet Bending Process," *J. Mater. Process. Technol.*, Vol. 60, pp. 225–232 (1996).

[2] Samuel, M., "Experimental and Numerical Prediction of Springback and Side Wall Curl in U-Bendings of Anisotropic Sheet Metals," *J. Mater. Process. Technol.*, Vol. 105, pp. 382–393 (2000).

[3] Liu, G., Lin, Z., Xu, W. and Bao, Y., "Variable Blankholder Force in U-Shaped Part Forming for Eliminating Springback Error," *J. Mater. Process. Technol.*, Vol. 120, pp. 259–264 (2002).

[4] Chan, W. M., Chew, H. I., Lee, H. P. and Cheok, B. T., "Finite Element Analysis of Spring-Back of V-Bending Sheet Metal Forming Processes," *J. Mater. Process. Technol.*, Vol. 148, pp. 15–24 (2004).

[5] Ling, Y. E., Lee, H. P. and Cheok, B. T., "Finite Element Analysis of Springback in L-Bending of Sheet Metal," *J. Mater. Process. Technol.*, Vol. 168, pp. 296–302 (2005).

[6] Lin, J. C. and Tai, C. C., "The Application of Neural Networks in the Prediction of Spring-Back in an L-Shaped Bend," *Int. J. Adv. Manuf. Technol.*, pp. 163–170 (1999).

[7] Gan, W. and Wagoner, R. H., "Die Design Method for Sheet Springback," *Int. J. Mech. Sci.*, Vol. 46, pp. 1097–1113 (2004).

[8] Sousa, L. C., Castro, C. F. and Antònio, C. A. C., "Optimal Design of V and U Bending Process Using Genetic Algorithms," *J. Mater. Process. Technol.*, Vol. 172, pp. 35–41 (2006).

[9] Jang, J. S. R., "ANFIS: Adaptive-Network-Based Fuzzy Inference System," *IEEE Trans. Syst. Man. Cybern.*, Vol. 23, pp. 665–685 (1993).

[10] Lu, Y. H., Yeh, F. H., Li, C. L. and Wu, M. T., "Study of Using ANFIS to the Prediction in the Bore-Expanding Process," *Int. J. Adv. Manuf. Technol.*, Vol. 26, pp. 544–551 (2005).

[11] Yeh, F. H., Lu, Y. H., Li, C. L. and Wu, M. T., "Application of ANFIS for Inverse Prediction of Hole Profile in the Square Hole Bore-Expanding Process," *J. Mater. Process. Technol.*, Vol. 173, pp. 136–144 (2006).

[12] Yeh, F. H., Wu, M. T. and Li, C. L., "Accurate Optimization of Blank Design in Stretch Flange Based on a Forward – Inverse Prediction Scheme," *Int. J. Mach. Tool. Manu.*, Vol. 47, pp. 1854–1863 (2007).

[13] ANSYS/LS-DYNA Theoretical Manual. ANSYS Inc., Canonsburg, PA (2006).

[14] Takagi, T. and Sugeno, M., "Derivation of Fuzzy Control Rules from Human Operator's Control Actions," *Proceedings of IFAC Symposium on Fuzzy Information, Knowledge Representation and Decision Analysis*, pp. 55–60 (1983).

Manuscript Received: Mar. 8, 2011
Accepted: Sep. 16, 2011